Pressure Sensitivity of Side-Hole Optical Fiber Sensors

J. R. Clowes, S. Syngellakis, and M. N. Zervas, *Member, IEEE*

***Abstract*— The dependency of the pressure-induced birefringence of a side-hole fiber on its geometry has been numerically investigated using the finite element method. We demonstrate that the pressure sensitivity of such a fiber shows a linear dependence on φ^2, where φ is the angle between the side hole center and core center axis and the core center to side-hole tangent. Experimental data obtained with two different side-hole fiber sensors are shown to agree extremely well (to within 1%) with theoretical predictions.**

***Index Terms*—Birefringence, optical fibers, pressure measurement.**

I. Introduction

SIDE-HOLE fiber was proposed by Xie *et al.* [1] as a possible sensor for hydrostatic or acoustic pressure. In the presence of hydrostatic pressure acting on the fiber surface, an anisotropic stress is induced in the core due to the fiber geometry. Through the photoelastic effect, the result is a pressure-induced birefringence which is a direct measure of the applied pressure.

In this letter, we will present experimental data for pressure sensors fabricated from two different geometries of side-hole fiber. We monitor the pressure-induced birefringence in the two sensors and calculate the pressure sensitivity of various fiber geometries. The measurements are performed at low temperature to avoid the recently observed drifts in fiber birefringence in high pressure fluid environments [2].

Using the finite-element method (FEM), the two geometries of side-hole fiber are modeled and a comparison is drawn between theory and experiment to show excellent correlation in the pressure sensitivities.

Finally, using the developed FEM model, we investigate the dependence of the pressure sensitivity of side-hole fiber upon the fiber geometry.

II. Polarimetric Fiber Pressure Sensor

Fig. 1 shows schematically the experimental setup used to measure the birefringence of the side-hole fibers. The sensor head consists of an input fiber polarizer aligned at 45° to the birefringent axes of a length of side-hole fiber (typically between 0.15 and 0.3 m in length). A mirror-ended fiber is spliced to the end of the sensor to increase the reflected power.

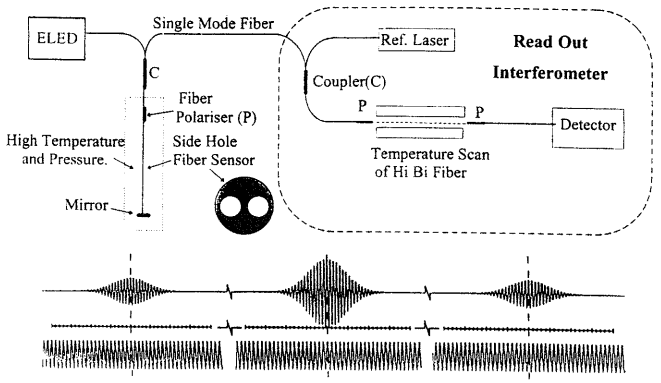

Fig. 1. Schematic of the experimental setup used to measure the pressure-induced birefringence in side-hole fiber and a typical output fringe pattern.

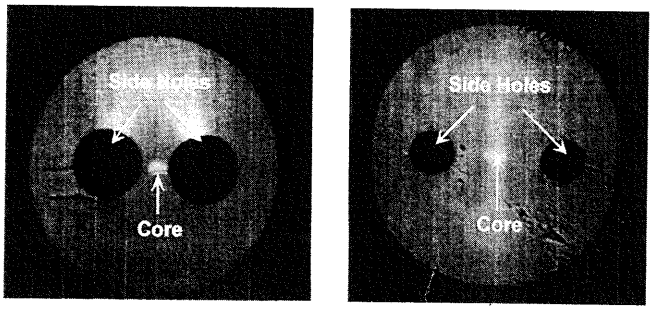

(a) (b)

Fig. 2. Cross-section photographs of (a) fiber A and (b) fiber B.

The pressure-induced birefringence in the sensing head is remotely monitored using a matched low-coherence interferometer in which the path difference is matched in a reference Hi-Bi fiber scanned in temperature [3]. The number of fringes between the central and side peaks in the resulting fringe pattern (Fig. 1) is a direct measure of the pressure-induced retardation. All measurements were made at 1300 nm and hydrostatic pressure was applied to the fiber by means of a dead-weight tester through a liquid medium.

III. Experimental Results

Fig. 2 shows photographs of two different side-hole fiber geometries that have been used in pressure sensor measurements. The dimensions of the structure are given in Table I

Manuscript received December 23, 1997; revised March 3, 1998. This work was supported by Sensor Dynamics and by Chevron.

J. R. Clowes and M. N. Zervas are with the Optoelectronics Research Centre, University of Southampton, Southampton, Hampshire, SO17 1BJ, U.K.

S. Syngellakis is with the Department of Mechanical Engineering, University of Southampton, Southampton, Hampshire, SO17 1BJ, U.K.

Publisher Item Identifier S 1041-1135(98)03786-0.

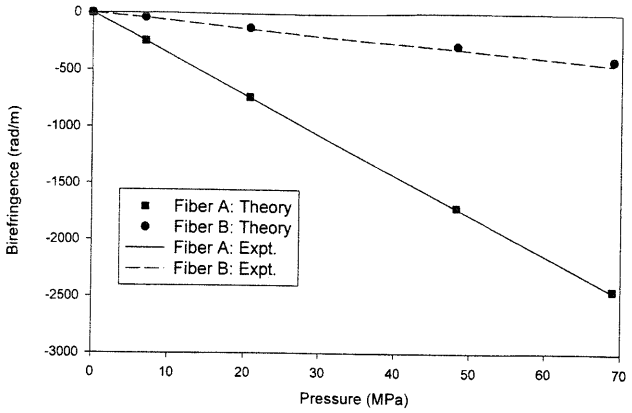

Fig. 3. Predicted and measured pressure-induced birefringence of fiber A and fiber B.

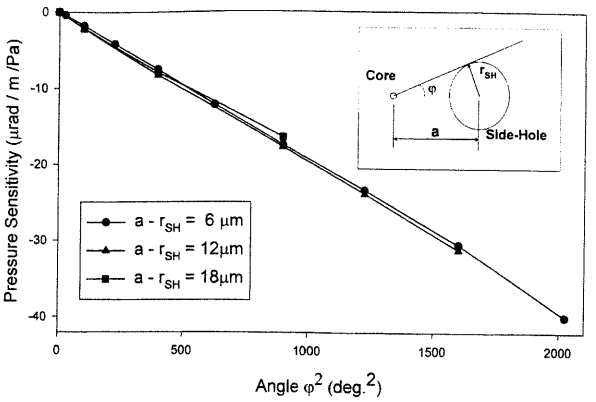

Fig. 4. Predicted pressure-induced birefringence versus φ^2 for three fibers with core to side-hole separations of 6, 12, and 18 μm. Inset: Schematic of the fiber geometry.

TABLE I
SUMMARY OF FIBER GEOMETRY PARAMETERS AND SENSITIVITY RESULTS

Fiber	a(μm)	r_{SH} (μm)	φ(deg.)	Sensitivity (μrad/m/Pa)
A(Theory)	24.46	16.49	42.39	35.69
B(Theory)	9.50	30.0	18.46	6.51
A (Expt.)	≈24.46	≈16.49	≈42.39	35.41
B (Expt.)	≈ 9.50	≈30.0	≈18.46	5.91

where r_{SH} is the side hole radius, a is the distance between the core and side-hole centers and φ is the angle between the side-hole center and core center axis and the core center to side-hole tangent (see the inset of Fig. 4). The fibers were fabricated to be 125 μm in diameter although it is clear that there has been considerable distortion and hole collapse in fiber B during the fiber pulling procedure. Fiber A clearly has a better circularity than fiber B although there is a small amount of core ellipticity in this example as well.

Fig. 3 shows the measured birefringence of fibers A and B with applied pressure. Note that any intrinsic (zero pressure) fiber birefringence due to core ellipticity and fiber residual stresses has been ignored.

The relationship for both fibers is a linear one with pressure although the two fiber sensitivities (given in Table I) differ considerably. It can be noted that the fiber with large side-holes is the more sensitive of the two by a factor of approximately 6.

IV. THEORY: FINITE-ELEMENT MODEL

FEM can be used to predict the localized pressure-induced stresses $(\sigma_{x,y,z})$ in the side-hole fiber from which the localized refractive index perturbations (Δn_x, and Δn_y) may be calculated by the photoelastic equations [4]. Assuming that the stress-induced perturbation of the refractive index is small $(\Delta n_{x,y} \ll n_0)$, an expression may be derived to describe the modal distribution within a perturbed fiber in terms of known modes in an unperturbed weakly guiding fiber [5]. With an invariant longitudinal perturbation, the change in propagation constant may be described by

$$\beta_{x,y} = \overline{\beta} + k\frac{\left[\int_{A_\infty} (n_{x,y} - n_0)E^2\, dA\right]}{\int_{A_x} E^2\, dA}. \quad (1)$$

Here, $\beta_{x,y}$ are the perturbed propagation constants in the x- and y-polarization directions and $\overline{\beta}$ is the unperturbed propagation constant. $n_{x,y}$ are the perturbed refractive indexes in the x- and y-polarization directions and n_0 is the unperturbed refractive index of the material. $k = 2\pi/\lambda$, where λ is the free-space wavelength. A is the area of the fiber cross section and E describes the electric field distribution. The fiber birefringence can therefore be calculated simply using the expression $\Delta\beta = \beta_x - \beta_y$ (in rad/m).

The fiber has been modeled as closely as possible to a side-hole fiber manufactured from a standard telecommunications grade preform; fiber radius $r_f = 62.5$ μm, core radius $r_c = 4$ μm, cladding Young modulus $E_{cl} = 72$ GPa and Poisson ratio $\nu_{cl} = 0.173$, the 3% germanium-doped core Young modulus $E_c = 70.8$ GPa and Poisson ratio $\nu_c = 0.165$ [6]. Values of the strain optic coefficients of silica (P_{11} and P_{12}) of 0.121 and 0.27 have been used in the analysis.

A two-dimensional stress analysis was performed using ANSYS, a general-purpose FEM package [7]. The FEM output includes the centroid coordinates, the area and the x and y normal stresses for every element. Calculation of the birefringence is therefore achieved by calculating $\Delta n_{x,y}$ for each element using the photoelastic equations, calculating the respective field magnitude for each element and finally evaluating β_x and β_y from (1).

The model uses parameters for a standard telecommunications-grade fiber with a numerical aperture of 0.12, core

index of 1.462, and a cladding index of 1.457. The operating wavelength is taken to be 1300 nm.

V. Numerical Results

The solid and dashed lines of Fig. 3 show the modeled birefringence versus applied pressure for fiber geometries A and B, respectively. This result shows excellent agreement between the model and experiment for fiber A (to approximately 99% accuracy). For fiber B, an accuracy of approximately 91% is achieved. Here, the larger discrepancy can be attributed to the noncircular fiber, hole and core shapes which are consequences of side-hole collapse during fiber fabrication.

A simple observation of the results of Fig. 3 shows that the fiber with large holes (fiber A) has a much greater sensitivity to pressure (approximately 6 times) than a fiber with small holes separated a greater distance from the core (fiber B). The model has therefore been utilized to investigate the relationship between the side-hole position and size and the pressure sensitivity of the fiber.

Side-hole fibers with the same hole position $(a\text{-}r_{SH})$ but varying hole radius (r_{SH}) have been modeled using values for the core to side-hole separation $(a\text{-}r_{SH})$ of 6, 12, and 18 μm. By varying the side-hole radius and location, the angle φ (see inset of Fig. 4) is effectively being varied. Fig. 4 shows the results for the pressure induced birefringence of the three cases mentioned when plotted against φ^2. The curves all show that the pressure sensitivity of the fiber follows a highly linear relationship with φ^2 for values of φ up to approximately 45°. Examination of the fibers A and B and their respective values of φ suggests that fiber A should have approximately 5.3 times the pressure sensitivity as fiber B. The actual measured value is about six times. However, the FEM analysis has considered fiber cross sections of perfect cladding and core circularity which is obviously not true for fiber B and to a lesser extent, fiber A.

Fig. 4 also shows that the sensitivity of the fiber is not significantly affected by the positioning of the holes as all three lines have a very similar gradient. This is an extremely interesting and useful result in terms of the manufacturing of such fibers. It suggests that a fiber with small holes near to the core will have a high-pressure sensitivity. This will make it possible to fabricate a highly pressure sensitive side-hole fiber whilst maintaining a relatively strong structure.

VI. Conclusion

We have modeled the pressure sensitivity of side-hole fiber sensors using the method of finite elements and have shown excellent agreement between the model results and side-hole fibers used in laboratory high pressure experiments. By investigating various geometries of side-hole fiber, the model predicts a linear relationship between pressure sensitivity and φ^2, where φ is the angle between the side-hole center and core center axis and the core center to side-hole tangent. This relationship has not been investigated analytically but is shown to be true for any side-hole fiber geometry having a value of φ up to 45°. Fibers having values of φ greater than 45° tended to deviate from the straight line relationship. However, such fiber geometries would be extremely fragile and therefore impractical. Two fibers used in laboratory pressure measurements with values of φ of 42.39 and 18.46°, show a very good agreement with the φ^2 relationship. Any discrepancy (of approximately 10% in the worst case) is attributed to core and fiber noncircularities. Finally, we predict that a highly pressure-sensitive fiber may be fabricated with small holes located close to the core to maintain fiber strength and integrity.

Acknowledgment

Helpful discussions with Prof. D. N. Payne, Dr. E. Kluth, and Dr. M. P. Varnham are gratefully acknowledged.

References

[1] H. M. Xie, Ph. Dabkiewicz, R. Ulrich, and K. Okamoto, "Side-hole fiber for fiber-optic pressure sensing," *Opt. Lett.*, vol. 11, no. 5, pp. 333–335, 1986.

[2] J. R. Clowes, J. McInnes, M. N. Zervas, and D. N. Payne, "Effects of high temperature and pressure on silica optical fiber sensors," *IEEE Photon. Technol. Lett.*, vol. 10, pp. 403–405, Mar. 1998.

[3] M. G. Xu, M. Johnson, M. Farhadiroushan, and J. P. Dakin, "Novel polarimetric fiber device for interrogating white-light interferometers," *Electron. Lett.*, vol. 29, no. 4, pp. 378–379, 1993.

[4] A. Yariv and P. Yeh, *Optical Waves in Crystals*. New York: Wiley, 1984, ch. 9.

[5] A. W. Snyder and J. D. Love, *Optical Waveguide Theory*. London, U.K.: Chapman & Hall, 1983, pp. 375–376.

[6] N. P. Bansal, *Handbook of Glass Properties*. London, U.K.: Academic, 1986.

[7] ANSYS User's Manual for Revision 5.1—Volumes I–IV, Swanson Analysis Systems, Housten, PA, 1994.